Low-Harmonic-Contents and High-Efficiency Class E Full-Wave Current-Driven Rectifier for Megahertz Wireless Power Transfer Systems

Ming Liu, *Student Member, IEEE*, Minfan Fu, *Student Member, IEEE*, and Chengbin Ma, *Member, IEEE*

***Abstract*—Wireless power transfer (WPT) working at megahertz (MHz) is now being widely considered a promising candidate for the midrange transfer of a medium amount of power. Efforts have been made to build high-efficiency MHz WPT systems via both component- and system-level approaches. However, so far there have been few discussions on high-frequency rectifier for MHz WPT applications. The soft-switching-based rectifiers, such as the Class E rectifiers, are one of the promising candidates for MHz rectification. This paper investigates the application of a Class E full-wave current-driven rectifier, for the first time, in WPT systems. A procedure is also developed to optimize the design of the rectifier and the MHz WPT system. For comparison purposes, the performances of both the Class E rectifier and the conventional full-bridge rectifier are investigated in terms of total harmonic distortion (THD), efficiency, power factor, voltage/current stresses, and voltage/current transfer functions, when being applied in an example 6.78-MHz WPT system. The simulation and experimental results show that the input voltage THD of the Class E full-wave rectifier is reduced to one-fourth of the THD of the full-bridge rectifier. In the optimally designed MHz WPT system, efficiencies of both the rectification (over 91%) and the overall system (around 80%) are obviously improved compared to the system using the conventional full-bridge rectifier.**

***Index Terms*—Class E full-wave current-driven rectifier, efficiency, low-harmonic contents, megahertz wireless power transfer (MHz WPT).**

I. Introduction

THERE is now a dramatic need in charging various electronic devices (e.g., cellphones, laptop computers, wearable devices, medical implant devices, etc.) and other high-power systems, especially electric vehicles. This need makes the wireless power transfer (WPT) using inductive resonance coupling, i.e., the so-called inductive coupling and magnetic resonance coupling, increasingly popular in recent years [1], [2]. Currently WPT working at kilohertz (kHz) is making significant progress in power level, system design, and applications [3]–[7]. Meanwhile, for medium- and low-power applications, further increasing the resonance frequency such as to several megahertz (MHz) brings a higher level of spatial freedom, namely a longer transfer distance and higher tolerance to coupling coil misalignment, and is desirable for building more compact and lighter WPT systems [2], [8]. Now WPT working at MHz is being widely considered a promising candidate for the midrange transfer of a medium amount of power. Meanwhile, in MHz WPT systems, ultrahigh-speed logic gates are required to drive the MOSFET switches. This leads to increased gate power dissipation and cost. The soft-switching operation of the power amplifier (PA) and the rectifier is also expected to reduce the increased switching losses [9], [10]. Besides, generally the parasitic resistances of the ac inductors including the coupling coils increase at MHz. It is especially desirable to use high-Q (quality factor) inductors and coupling coils for conduction loss reduction [11]. Moreover, the impedance characteristics of circuits working at MHz are much more complicated than those at kHz. For instance, at MHz, the influence of the parasitic and/or parallel capacitors of the diodes becomes significant. This causes nonneglectable reactance of the rectifier that could lower the efficiency and power transfer capability of the system [12]. In addition, electromagnetic interference (EMI) problem in the MHz WPT systems is also more challenging. In order to improve the overall performance of the MHz WPT systems, it is important to introduce new topologies of the circuits, and conduct comprehensive analysis and optimization.

Efforts have been made to build high-efficiency MHz WPT systems via both component- and system-level approaches focusing on the improvements in coupling coils [13]–[17], PA [18]–[21], and load control [22]–[24]. At the same time, so far there have been few discussions on high-frequency rectifier for MHz WPT applications. Most existing MHz WPT systems use conventional hard-switching-based rectifiers such as the full-bridge rectifier. Due to the hard-switching operation, there is significant switching loss from the full-bridge rectifier when operating at MHz. In addition, the hard switching also leads to high-voltage harmonic contents in WPT systems due to the square-wave input voltage in the full-bridge rectifier. For a high-frequency rectification at MHz, the soft-switching-based rectifiers, such as the Class E rectifiers, are one of the promising candidates. Meanwhile, care should be taken to use proper diodes due to the higher diode voltage stress in the Class E rectifiers [25]. The Class E rectifier was first proposed for a high-frequency dc–dc converter in 1988 [26]. Various Class E

Manuscript received September 30, 2015; revised January 16, 2016; accepted March 28, 2016. Date of publication April 6, 2016; date of current version November 11, 2016. This work was supported by Shanghai Natural Science Foundation under Grant 16ZR1416300. Recommended for publication by Associate Editor M. A. E. Andersen.

M. Liu and M. Fu are with the University of Michigan-Shanghai Jiao Tong University Joint Institute, Shanghai Jiao Tong University, Minhang, Shanghai 200240, China (e-mail: mikeliu@sjtu.edu.cn; fuminfan@sjtu.edu.cn).

C. Ma is with the University of Michigan-Shanghai Jiao Tong University Joint Institute, Shanghai Jiao Tong University, Shanghai 200240, China, and also with the School of Mechanical Engineering, Shanghai Jiao Tong University, Shanghai 200240, China (e-mail: chbma@sjtu.edu.cn).

Color versions of one or more of the figures in this paper are available online at http://ieeexplore.ieee.org.

Digital Object Identifier 10.1109/TPEL.2016.2551288

topologies were later reported including voltage/current-driven and half-wave/full-wave ones [27]–[32].

The research on high-frequency rectification in WPT system is relatively new. Among the following few existing references, [33] discussed, for the first time, the application of the Class E rectifier in a 800-kHz WPT system. In [33], a piecewise linear state-space representation is used to model and design the Class E rectifier. A 200-kHz Class E^2 WPT system was later built, i.e., a combination of a Class E PA and a Class E rectifier [34]. Initial discussions on applying the Class E rectifier in MHz WPT systems can be found in [35] and [36], where the real implementation and the simulation-based analysis of the Class E rectifiers were introduced, respectively. Liu *et al.* [25] reported new progress on the system-level optimization of a 6.78-MHz WPT using the Class E rectifier. In the above references, all the Class E rectifiers are half-wave, and thus, their input current or voltage waveforms are nonsinusoidal and asymmetric. This disadvantage causes high harmonic contents in the input voltage/current of the rectifiers, and thus, adversely influences the efficiency and EMI performance of the MHz WPT systems. It is known that the input voltage/current harmonic contents of the rectifier can disrupt the resonant operation of the coupling coils and the Class E PA [33], and poor EMI performance may affect other nearby electronic devices and eventually limit the usage of the WPT system. Thus, it is important to investigate and develop a low-harmonic-contents and high-efficiency rectifier that targets the applications in MHz WPT.

This paper investigates the application of a Class E full-wave current-driven rectifier, for the first time, in MHz WPT systems, particularly the optimized design of the overall WPT system when using the rectifier. Because of the sinusoidal input voltage and current, this soft-switching-based rectifier is a promising candidate for low-harmonic-contents and high-efficiency rectification at MHz. Based on the newly derived input impedance of the Class E full-wave rectifier, the parameters of the coupling coils and the PA are further optimized for a high efficiency of the overall WPT system. For comparison purposes, the performances of both the Class E rectifier and the conventional full-bridge rectifier are investigated in terms of total harmonic distortion (THD), efficiency, power factor, voltage/current stresses, and voltage/current transfer functions, when being applied in an example 6.78-MHz WPT system. The simulation and experimental results show that the input voltage THD of the Class E full-wave rectifier is reduced to one-fourth of the THD of the full-bridge rectifier. In the optimally designed MHz WPT system, efficiencies of both the rectification (over 91%) and the overall system (around 80%) are obviously improved compared to the system using the conventional full-bridge rectifier.

II. Class E Full-Wave Rectifier

The circuit model of the Class E full-wave current-driven rectifier is shown in Fig. 1. The current-driven topology is chosen because it can be applied both in parallel–series and series–series WPT systems. The rectifier consists of two filter inductors L_1 and L_2, two parallel capacitors C_1 and C_2 with an identical capacitance C, two rectifying diodes D_1 and D_2, a

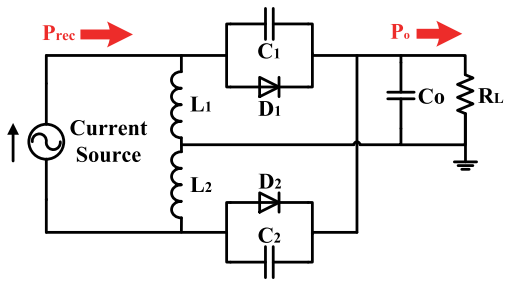

Fig. 1. Circuit model of the Class E full-wave current-driven rectifier.

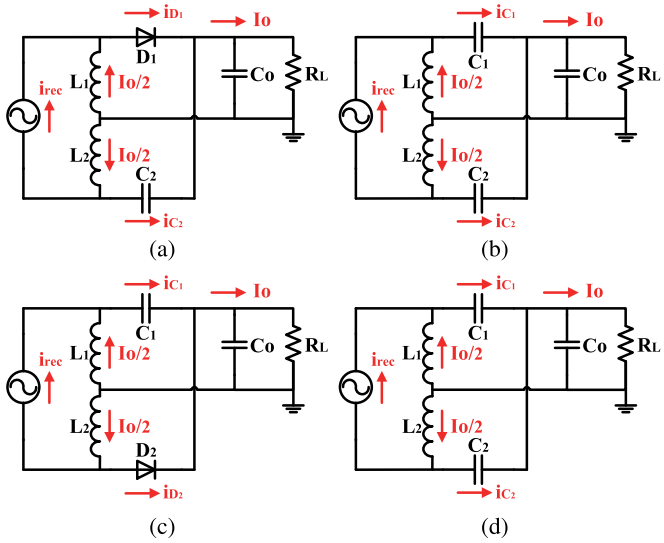

Fig. 2. Operating modes of Class E full-wave rectifier. (a) D_1 ON and D_2 OFF. (b) D_1 OFF and D_2 OFF. (c) D_1 OFF and D_2 ON. (d) D_1 OFF and D_2 OFF.

filter capacitor C_o, and a dc load R_L. $P_{\rm rec}$ and P_o are the input/output power of the rectifier, respectively. In this paper, two silicon carbide diodes STPSC406 are used as the rectifying elements, and their parasitic capacitors are absorbed by the parallel capacitors. Fig. 2 shows four operating modes of the full-wave rectifier during one switching period. In the figure, the input current of the rectifier $i_{\rm rec}$ is sinusoidal; i_{D_1} and i_{D_2} are the currents through diode D_1 and D_2; i_{C_1} and i_{C_2} are the currents through C_1 and C_2; I_o is the dc output current of the rectifier. Since the inductances of L_1 and L_2 are equal and sufficiently large, the currents through the two inductors are equal to $I_o/2$. In the rectifier, i_{C_1} and i_{C_2} shape the waveforms of the voltages across D_1 and D_2, and thus turn on and off the two diodes. For example, as shown in Fig. 2(a), D_1 is turned ON, and D_2 is turned OFF. The currents $I_o/2 + i_{\rm rec}$ and $I_o/2 - i_{\rm rec}$ flow through D_1 and C_2, respectively. Because the current through the parallel combination of C_o and R_L is $(I_o/2+i_{\rm rec}) + (I_o/2 - i_{\rm rec})$, theoretically the output current of the rectifier is a pure dc. In real applications, the circuit cannot be completely symmetrical. The filter capacitor C_o is still needed, but its capacitance is much smaller than that in conventional rectifiers such as the full-bridge rectifier. The operations in the other three modes can be similarly explained.

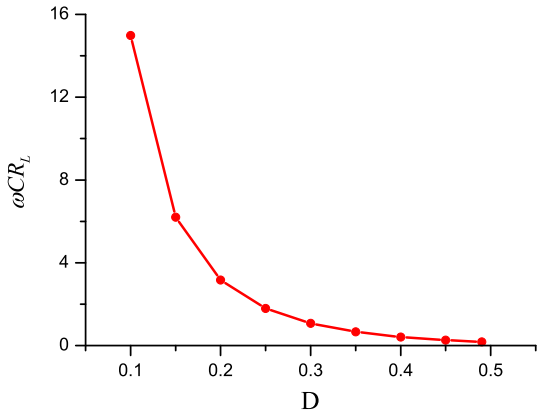

Fig. 3. Diode duty cycle D versus the normalized load resistance $\omega C R_L$.

In the Class E full-wave rectifier, C, the capacitance of the two parallel capacitors, is the only parameter that needs to be determined. C can be represented as follows [32]:

$$C = \frac{1}{\omega R_L}\left[\frac{1}{4\pi} - \frac{\pi}{2}(1-D)^2 + \frac{2\pi(1-D)\cos(\phi_{\rm rec}+2\pi D) - \sin\phi_{\rm rec}}{4\pi\sin(\phi_{\rm rec}+2\pi D)}\right] \quad (1)$$

and

$$\tan\phi_{\rm rec} = -\frac{\pi(1-D)\sin(2\pi D) + \sin^2(\pi D)}{\pi(1-D)\cos(2\pi D) + \sin(\pi D)\cos(\pi D)} \quad (2)$$

where ω is the operating frequency, D is the duty cycle of the two diodes, and $\phi_{\rm rec}$ is the initial phase of $i_{\rm rec}$. It can be seen from (1) and (2) that D is determined by the values of C and R_L assuming a fix ω. The Class E rectifier is usually designed to work at 50% duty cycle for a maximized power output capability. However, for the Class E full-wave rectifier, the overlapping of the diode conduction occurs when $D \geq 0.5$, i.e., D_1 and D_2 are both turned ON at the same time. Since the capacitors C_1 and C_2 are shorted out during the overlapping, the full-wave rectifier simply works as a hard-switching-based rectifier. This leads to higher harmonic contents and lower efficiency of the rectifier. Thus, in this paper, the maximum duty cycle of the diodes is chosen as 0.49 to avoid the overlapping and maximize the power output capability of the rectifier. Fig. 3 shows the relationship between the normalized load resistance $\omega C R_L$ and duty cycle D. It can be seen that a smaller R_L will lead to a higher D when ω and C are fixed. In order to have D smaller than 0.49, C should be determined by the minimum target value of R_L, $R_{L,\rm min}$. Thus, the optimal C, $C_{\rm opt}$, can be calculated by letting $D = 0.49$ and $R_L = R_{L,\rm min}$ in (1) and (2)

$$C_{\rm opt} = \frac{0.1756}{\omega R_{L,\rm min}}. \quad (3)$$

In order to optimize the overall MHz WPT systems, it is important to derive the input impedance of the Class E full-wave rectifier $Z_{\rm rec}$, which can be represented as

$$Z_{\rm rec} = R_{\rm rec} + jX_{\rm rec} \quad (4)$$

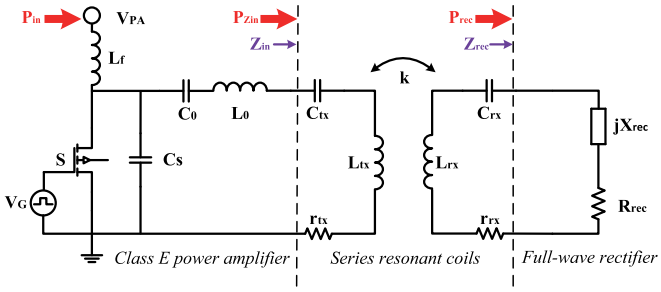

Fig. 4. Circuit model of the WPT system with $Z_{\rm rec}$.

where $R_{\rm rec}$ is the resistance and $X_{\rm rec}$ is the reactance. Following the derivation procedure in [25], the input impedance of the Class E full-wave rectifier is newly derived as follows assuming that the diodes and inductors are ideal components. Note the derived input impedance here is different from that of the full-wave rectifier derived in [32], where the rectifier is driven by two symmetrical current sources. The below input impedance of the rectifier serves as the basis for the following parameter design of the coupling coils and the Class E PA that maximizes the overall efficiency of the WPT system

$$R_{\rm rec} = \frac{2\sin(\phi_{\rm rec}+2\pi D)}{\pi\omega C_{\rm opt}}\left[\sin(\phi_{\rm rec}+2\pi D) - \sin\phi_{\rm rec} + 2\pi(1-D)\cos\phi_{\rm rec} + \frac{\cos\phi_{\rm rec} - \cos(\phi_{\rm rec}+2\pi D)}{4\sin(\phi_{\rm rec}+2\pi D)} + \frac{\cos 2(\phi_{\rm rec}+2\pi D) - \cos 2\phi_{\rm rec}}{\tan(\phi_{\rm rec}+2\pi D)}\right] \quad (5)$$

and

$$X_{\rm rec} = -\frac{2\sin(\phi_{\rm rec}+2\pi D)}{\pi\omega C_{\rm opt}}\left[\cos\phi_{\rm rec} + 2\pi(1-D)\sin\phi_{\rm rec} - \frac{\sin\phi_{\rm rec}}{\tan(\phi_{\rm rec}+2\pi D)} - \frac{\cos(\phi_{\rm rec}+2\pi D)}{2} + \frac{2\pi(1-D) + \sin\phi_{\rm rec}\cos\phi_{\rm rec}}{2\sin(\phi_{\rm rec}+2\pi D)}\right]. \quad (6)$$

III. System Parameter Design

Here, the parameter design procedure of an example 6.78-MHz WPT system is discussed and developed based on the input impedance of the rectifier derived in Section II. Fig. 4 shows the circuit model of the WPT system, which includes a Class E PA, coupling coils, and the Class E full-wave rectifier. In the figure, $P_{\rm in}$ is the input power of the PA, $P_{Z_{\rm in}}$ is the input power of coupling coils, and $Z_{\rm in}$ is the input impedance of coupling coils.

A. Coupling Coils

In the conventional WPT systems using the full-bridge rectifier, the coupling coils are compensated to be resonant at a target frequency by the compensation capacitors. However, the input reactance of the full-bridge rectifier is usually neglected

because it is difficult to analytically derive the input impedance of the full-bridge rectifier. It is known that the input reactance of the rectifiers becomes obvious at MHz such as the full-bridge rectifier [12]. Thus, the coupling coils are not accurately tuned to be fully resonant, which may affect the efficiency and power transfer capability of the coupling coils. In this paper, the derived input impedance of the full-wave rectifier, (5) and (6), is used to achieve a resonance exactly at a target frequency. The optimal compensation capacitors $C_{\mathrm{rx,opt}}$ and $C_{\mathrm{tx,opt}}$ should be determined following the below relationship:

$$j\omega L_{\mathrm{rx}} + \frac{1}{j\omega C_{\mathrm{rx,opt}}} + jX_{\mathrm{rec}} = 0 \tag{7}$$

$$j\omega L_{\mathrm{tx}} + \frac{1}{j\omega C_{\mathrm{tx,opt}}} = 0 \tag{8}$$

where L_{tx} and L_{rx} are the inductances of the emitting and receiving coils, respectively, and ω is the resonance/operating frequency of the WPT system, i.e., 6.78 MHz here. Then, the optimal compensation capacitors can be expressed as

$$C_{\mathrm{rx,opt}} = \frac{1}{\omega(\omega L_{\mathrm{rx}} + X_{\mathrm{rec}})} \tag{9}$$

$$C_{\mathrm{tx,opt}} = \frac{1}{\omega^2 L_{\mathrm{tx}}}. \tag{10}$$

In addition, based on (7) and (8), and Fig. 4, the input impedance of coupling coils Z_{in} can be derived as

$$Z_{\mathrm{in}} = r_{\mathrm{tx}} + \frac{\omega^2 k^2 L_{\mathrm{tx}} L_{\mathrm{rx}}}{r_{\mathrm{rx}} + R_{\mathrm{rec}}} \tag{11}$$

where k is the mutual inductance coefficient; and r_{tx} and r_{rx} are the parasitic resistances of the transmitting and receiving coils, respectively. It can be seen that with the optimal compensation capacitors $C_{\mathrm{tx,opt}}$ and $C_{\mathrm{rx,opt}}$, Z_{in} becomes pure resistive, and the compensation does not depend on the relative position of the coupling coils, i.e., k [refer to (9) and (10)]. Note that in real applications, due to the uncertainty in the value of the dc load R_L, it is difficult to achieve such a desirable precise resonance. The above results are valid at a target operating point.

According to Fig. 4, the efficiency of the coupling coils is defined as

$$\eta_{\mathrm{coil}} = \frac{P_{\mathrm{rec}}}{P_{Z_{\mathrm{in}}}} \tag{12}$$

where $P_{Z_{\mathrm{in}}}$ is the input power of the transmitting coil, and P_{rec} is the input power of the rectifier. The power loss occurs on the parasitic resistances of the coils, i.e., r_{tx} and r_{rx}. Thus, η_{coil} can be rewritten as

$$\eta_{\mathrm{coil}} = \frac{\mathrm{Re}\{Z_{\mathrm{in}}\} - r_{\mathrm{tx}}}{\mathrm{Re}\{Z_{\mathrm{in}}\}} \cdot \frac{R_{\mathrm{rec}}}{r_{\mathrm{rx}} + R_{\mathrm{rec}}} \tag{13}$$

where $\mathrm{Re}\{*\}$ means the real part of a complex number. Substituting (11) into (13) gives the efficiency of the coupling coils

$$\eta_{\mathrm{coil}} = \frac{\omega^2 k^2 L_{\mathrm{tx}} L_{\mathrm{rx}} R_{\mathrm{rec}}}{(\omega^2 k^2 L_{\mathrm{tx}} L_{\mathrm{rx}} + r_{\mathrm{tx}} r_{\mathrm{rx}} + r_{\mathrm{tx}} R_{\mathrm{rec}})(r_{\mathrm{rx}} + R_{\mathrm{rec}})}. \tag{14}$$

TABLE I
PARAMETERS IN COIL EFFICIENCY CALCULATION

R_{rec}	r_{tx}	r_{rx}	L_{tx}	L_{rx}
30 Ω	0.8 Ω	0.8 Ω	3.34 μH	3.34 μH

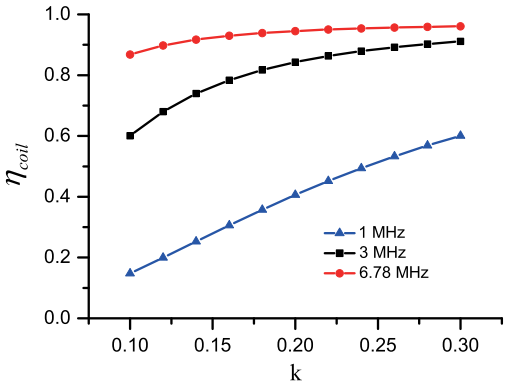

Fig. 5. Efficiency of the coupling coils versus k.

The above equation can be further written as

$$\eta_{\mathrm{coil}} = \frac{R_{\mathrm{rec}}}{(1 + \frac{r_{\mathrm{tx}} r_{\mathrm{rx}} + r_{\mathrm{tx}} R_{\mathrm{rec}}}{\omega^2 k^2 L_{\mathrm{tx}} L_{\mathrm{rx}}})(r_{\mathrm{rx}} + R_{\mathrm{rec}})}. \tag{15}$$

Thus, the efficiency of the coupling coils relates to the operating frequency ω, the mutual inductance coefficient k, and the inductances of the coils L_{tx} and L_{rx}. k indicates the required power transfer distance and the coil misalignment. Larger the transfer distance and coil misalignment, lower k. Meanwhile, the size of a coil is mainly determined by its inductance. Smaller the size of the coils, smaller L_{tx} and L_{rx}. As shown in (15), with a higher ω, a same coil efficiency can be maintained using smaller size coils, i.e., smaller L_{tx} and L_{rx}. Under the parameters in Table I, the efficiencies of the coupling coils are calculated and shown in Fig. 5 when sweeping k at different operating frequencies, 1, 3, and 6.78 MHz. Note for the sake of simplicity, the parameters in Table I are assumed to be constant in the calculation. As same as predicted by (15), under the 6.78-MHz operating frequency, a same efficiency such as 87% in the figure can be maintained under a small k ($= 0.10$), namely a long transfer distance and/or a large coil misalignment. Overall, a high operating frequency such as several MHz can help to reduce the size and weight of the WPT systems as well as achieve a high level of spatial freedom in terms of the power transfer distance and the tolerance to the coil misalignment [2], [8].

B. Power Amplifier

In the WPT system, the coupling coils are driven by a Class E PA. As shown in Fig. 4, it consists of a dc supply V_{PA}, a radio frequency (RF) choke L_f, a switch S, a shunt capacitor C_S, a series capacitor C_0, and a series inductor L_0. Here, C_S and C_0 are the design parameters for the Class E PA, and L_f should be sufficiently large such that the ac current will not flow through it. In order to achieve zero-voltage switching and maximize the PA efficiency, it is known that (16) and (17) can be used to

determine C_S and C_0 [37]

$$C_S = \frac{0.1836}{\omega Z_{\rm in}} \tag{16}$$

$$C_0 = \frac{1}{\omega^2 L_0 - 1.1525\omega Z_{\rm in}}. \tag{17}$$

Substituting the derived $Z_{\rm in}$ (11) into (16) and (17) gives the optimal design parameters of the Class E PA

$$C_{S,\rm opt} = \frac{0.1836(R_{\rm rec} + r_{\rm rx})}{\omega(r_{\rm tx}r_{\rm rx} + R_{\rm rec}r_{\rm tx} + \omega^2 k^2 L_{\rm tx}L_{\rm rx})} \tag{18}$$

and

$$C_{0,\rm opt} = \frac{R_{\rm rec} + r_{\rm rx}}{(\omega^2 L_0 - 1.1525\omega r_{\rm tx})(R_{\rm rec} + r_{\rm rx}) - 1.1525\omega^3 k^2 L_{\rm tx}L_{\rm rx}}$$

respectively. As shown in the equations, $C_{S,\rm opt}$ and $C_{0,\rm opt}$ are determined by $R_{\rm rec}$ and k, and according to (1)–(5), $R_{\rm rec}$ itself relates to R_L and $C_{\rm opt}$. Thus, an optimal operation of the Class E PA depends on the values of R_L, $C_{\rm opt}$, and k, namely a system level optimization. Note as discussed above, $C_{\rm tx}$, C_0, $L_{\rm tx}$, and L_0 at the transmitting side are all independent parameters in order to facilitate the component-level analysis and discussion.

IV. Performance Analysis and Comparison

Here, the performance of the Class E full-wave rectifier in the 6.78-MHz WPT system is analyzed and compared with that of the conventional full-bridge rectifier. A well-known RF simulation tool, advanced design system from Agilent, is used to investigate and compare the performances of the two rectifiers. The Pspice models of diode STPSC406 and MOSFET SUD06N10 are used in the simulation. The optimal parameters derived above are applied when using the Class E full-wave rectifier, while for the WPT system using the full-bridge rectifier, the compensation capacitors $C_{\rm tx}$ and $C_{\rm rx}$ are determined as 165 pF through the conventional design approach, i.e.,

$$j\omega L_{\rm rx} + \frac{1}{j\omega C_{\rm rx}} = 0 \tag{19}$$

$$j\omega L_{\rm tx} + \frac{1}{j\omega C_{\rm tx}} = 0. \tag{20}$$

Note that unlike the Class E full-wave rectifier, it is challenging to analytically derive the input impedance of the full-bridge rectifier, which makes the optimized design and analytical calculation difficult.

For the 6.78-MHz WPT system in Fig. 6, its optimal design parameters C, $C_{\rm rx}$, $C_{\rm tx}$, C_S, and C_0 are calculated using (3), (9), (10), (18), and (19), respectively. The calculated results for an example dc load R_L (= 30 Ω) are listed in Table II, where $R_{L,\rm min}$ is assumed to be 10 Ω. In the following simulation, the performances of the Class E full-wave rectifier are investigated in detail including THD, waveforms of the input voltage/current, efficiency and power factor, diode voltage/current stress, and voltage/current transfer function. Note the results when using the conventional full-bridge rectifier are also colisted for comparison purposes. In the following simulation and experiments, the two rectifiers, the Class E full-wave and full-bridge rectifiers use same diodes (STPSC406), as listed in Fig. 6.

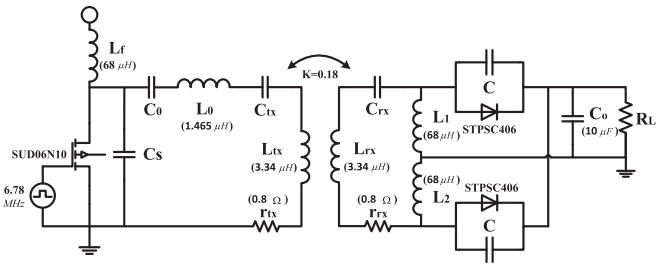

Fig. 6. Circuit model of the 6.78-MHz WPT system using the Class E full-wave rectifier.

TABLE II
Optimal Parameters When R_L (= 30 Ω) and k (= 0.18)

D	C	$C_{\rm rx}$	$C_{\rm tx}$	C_S	C_0
0.375	412 pF	265 pF	165 pF	187 pF	655 pF

A. Total Harmonic Distortion

Because the coupling coils and the Class E PA are originally designed to operate at resonance, the harmonic component of the input voltage/current of the rectifiers not only causes harmonic losses and heating problem in the receiving coil but also affects the performance and efficiency of both the coupling coils and the PA [33]. In addition, it causes poor EMI performance and, thus, adversely affects the operation of other nearby electronic devices. The input voltage/current THD of the rectifier can be used to evaluate the impact of rectifying operation on the signal quality of the WPT system. Due to the series resonant topology of the coupling coils here, the input current of the Class E full-wave current-driven rectifier is sinusoidal. Thus, the input voltage THD of the rectifier is investigated and compared with the full-bridge rectifier in the MHz WPT system. Here, THD is defined as

$$\text{THD} = \frac{\sqrt{\sum_{n=2}^{\infty} v^2_{{\rm rec},n}}}{v_{\rm rec,1}} \tag{21}$$

where $v_{\rm rec,1}$ is the fundamental component of the input voltage at the resonant frequency and $v_{{\rm rec},n}$ represents the *N*-order input voltage harmonics.

As shown in Fig. 7(a), (b), (d), and (e), the input currents of the two rectifiers are sinusoidal. The input voltage of the Class E full-wave rectifier is close to an ideal sinusoidal wave, while the input voltage of the full-bridge rectifier is a square wave. Fig. 7(c) and (f) gives the input voltage harmonic of the two rectifiers. It can be seen that the input voltage harmonic is much lower in the Class E full-wave rectifier than that in full-bridge rectifier. Note here only odd harmonics are shown for the two rectifiers due to the symmetrical topology. As shown in Fig. 7(c) and (f), the THD of the input voltage of the full-wave rectifier is 8.87%, about one-fourth of the THD of the full-bridge rectifier 37.5%. Using the Class E full-wave rectifier can significantly reduce the voltage harmonic contents in the MHz WPT system. In order to demonstrate the adverse influence of the diode conduction overlapping on the input voltage harmonic

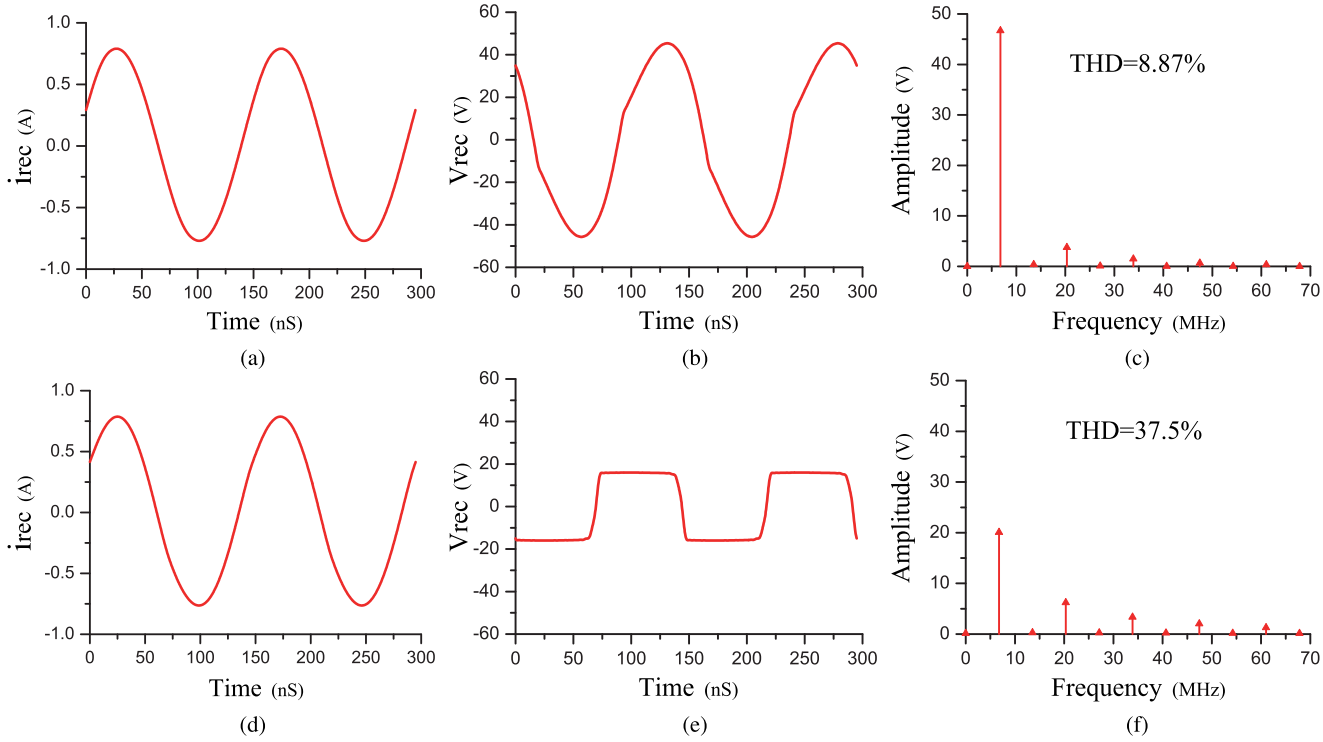

Fig. 7. Waveforms and harmonic contents. (a) Input current of the full-wave rectifier. (b) Input voltage of the full-wave rectifier. (c) Input voltage harmonic contents of the full-wave rectifier. (d) Input current of the full-bridge rectifier. (e) Input voltage of the full-bridge rectifier. (f) Input voltage harmonic contents of the full-bridge rectifier.

TABLE III
INPUT VOLTAGE THD WHEN $D > 0.5$

D	0.52	0.54	0.56	0.58	0.6
THD	13.7%	15.3%	19.7%	23.1%	27.8%

contents of the full-wave rectifier, Table III lists the input voltage THD of the rectifier when the overlapping occurs (duty cycle $D > 0.5$). It can be seen that a higher D, i.e., higher overlapping, leads to a higher input voltage THD. It is important to avoid the overlapping when using the full-wave rectifier, as discussed in Section II.

B. Efficiency and Power Factor

According to Fig. 1, the efficiency of the rectifier can be defined as

$$\eta_{\rm rec} = \frac{P_o}{P_{\rm rec}} \tag{22}$$

where P_o is the dc output power of the WPT system and $P_{\rm rec}$ is the input power of the rectifier. The efficiencies of the Class E full-wave rectifier and the full-bridge rectifier are given in Fig. 8(a) when R_L is swept from 10 to 100 Ω. The efficiency of the Class E full-wave rectifier is higher than that of the full-bridge rectifier over a wide range of R_L. Due to the soft-switching technique, the diodes in the Class E full-wave rectifier are turned ON and OFF at a low dv/dt and, thus, with low switching losses. In addition, since the waveforms of the current through the parallel combinations of C_1-D_1 and C_2-D_2 are the same sinusoidal waveforms and with 180° out of phase, the ac component in the output current is theoretically zero. This results in a nearly zero loss in the equivalent series resistance (ESR) of the filter capacitor C_0 in Fig. 1. Furthermore, the lower THD in the input voltage also indicates lower harmonic power loss. All the above advantages lead to a higher efficiency of the Class E full-wave rectifier over the conventional full-bridge rectifier.

The power loss breakdown for the Class E full-wave and full-bridge rectifiers are given in Table IV. For a fair comparison, the dc supply voltage of the PA $V_{\rm PA}$ is tuned to provide a same 10 W input power to the both rectifiers (i.e., $P_{\rm rec}$) when the target dc load R_L is 30 Ω. $P_{\rm sw}$ and $P_{\rm cd}$ are the switching loss and the diode conduction loss in two rectifiers, respectively. P_L is the loss from the two 68-μH dc filter inductors L_1 and L_2 in the full-wave rectifier. The power losses in the full-wave rectifier are calculated using the below equations, simulated dc output current I_o, and diode currents, i_{D_1} and i_{D_2} [refer to Fig. 2],

$$P_L = 2\left(\frac{I_o}{2}\right)^2 r_L \tag{23}$$

$$P_{\rm cd} = \frac{1}{2\pi}\left\{\int_0^{2\pi D}\left[V_F i_{D_1}(\omega t) + r_D i_{D_1}^2(\omega t)\right] d\omega t + \int_{2\pi(1-D)}^{2\pi}\left[V_F i_{D_2}(\omega t) + r_D i_{D_2}^2(\omega t)\right] d\omega t\right\} \tag{24}$$

$$P_{\rm sw} = P_{\rm rec} - P_o - P_L - P_{\rm cd} \tag{25}$$

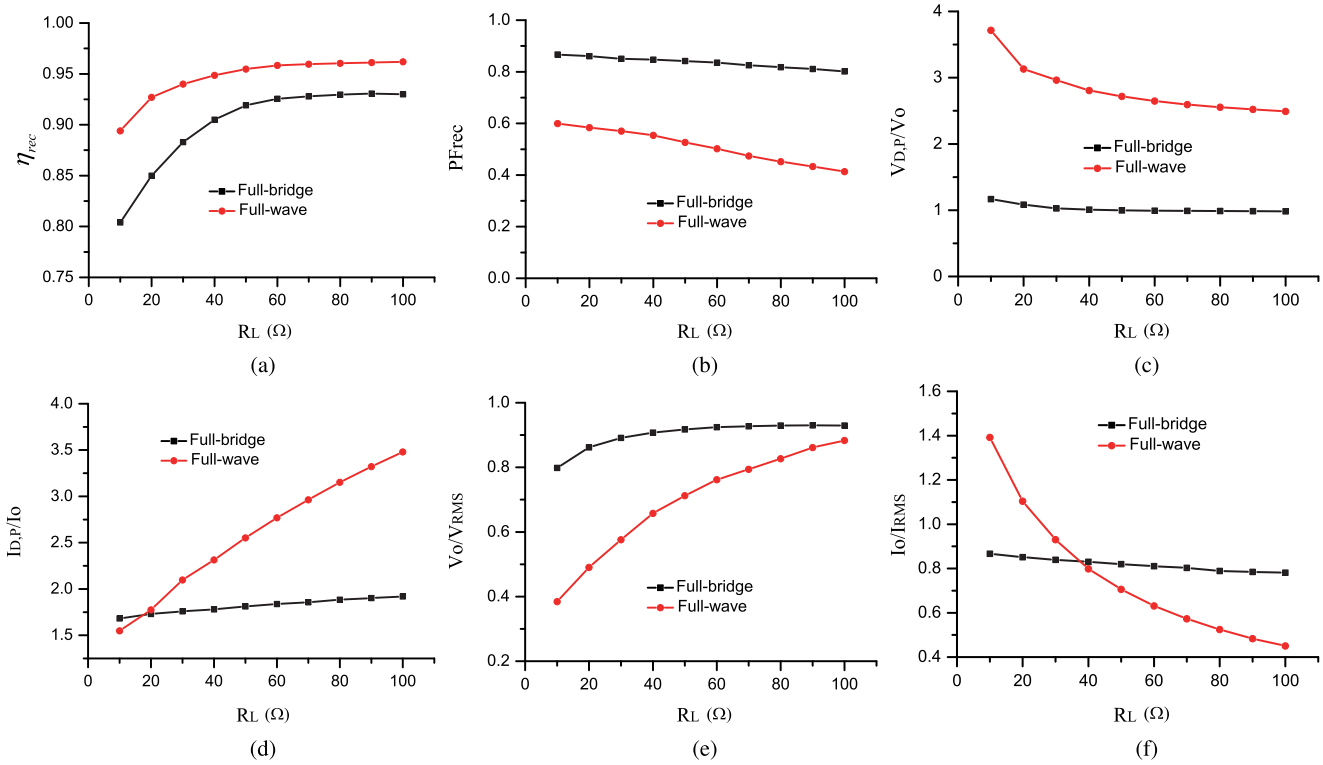

Fig. 8. Various parameters versus a varying R_L. (a) Efficiency. (b) Power factor. (c) Diode voltage stress. (d) Diode current stress. (e) Voltage transfer function. (f) Current transfer function.

TABLE IV
LOSS BREAKDOWN OF RECTIFIERS IN SIMULATION (RECTIFIER INPUT POWER $P_{\rm rec} = 10$ W; DC LOAD $R_L = 30\ \Omega$)

Loss	Full-wave Rec.	Full-bridge Rec.
$P_{\rm sw}$	0.28 W	0.61 W
$P_{\rm cd}$	0.29 W	0.59 W
P_L	0.03 W	–

TABLE V
$PF_{\rm dist}$ AND $\rm PF_{disp}$ OF RECTIFIERS IN SIMULATION ($R_L = 30\ \Omega$)

Power Factor	Full-wave Rec.	Full-bridge Rec.
$PF_{\rm dist}$	0.996	0.936
$PF_{\rm disp}$	0.573	0.909

where P_o is the dc output power of the WPT system; $P_{\rm rec}$ is the input power of the rectifier; r_L (= 0.2 Ω) is the ESR of the dc filter inductors L_1 and L_2; V_F (=1.2 V) is the forward voltage drop of the diodes, and r_D (= 0.3 Ω) is the on-resistance of the diodes. The power losses in the full-bridge rectifier can be similarly calculated

$$P_{\rm cd} = \frac{1}{2\pi}\left\{2\int_0^{\pi}\left[V_F i_{D_1}(\omega t) + r_D i_{D_1}^2(\omega t)\right]d\omega t + 2\int_{\pi}^{2\pi}\left[V_F i_{D_2}(\omega t) + r_D i_{D_2}^2(\omega t)\right]d\omega t\right\} \quad (26)$$

$$P_{\rm sw} = P_{\rm rec} - P_o - P_{\rm cd}. \quad (27)$$

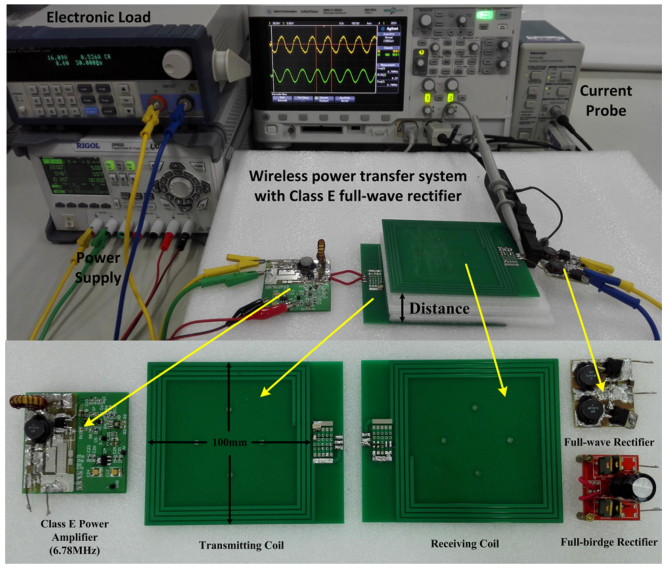

Fig. 9. Experimental setup of a 6.78-MHz WPT system.

Here, i_{D_1} and i_{D_2} are the diode currents at positive- and negative-half cycles, respectively. As shown in Table IV, the switching loss of the full-wave rectifier is lower than that of the full-bridge rectifier due to its low dv/dt switching. It is interesting to note that the conduction loss of the full-wave rectifier is also smaller. This is because the two diodes in the full-wave rectifier are not turned ON at the same time, while in the full-bridge rectifier two diodes are simultaneously turned

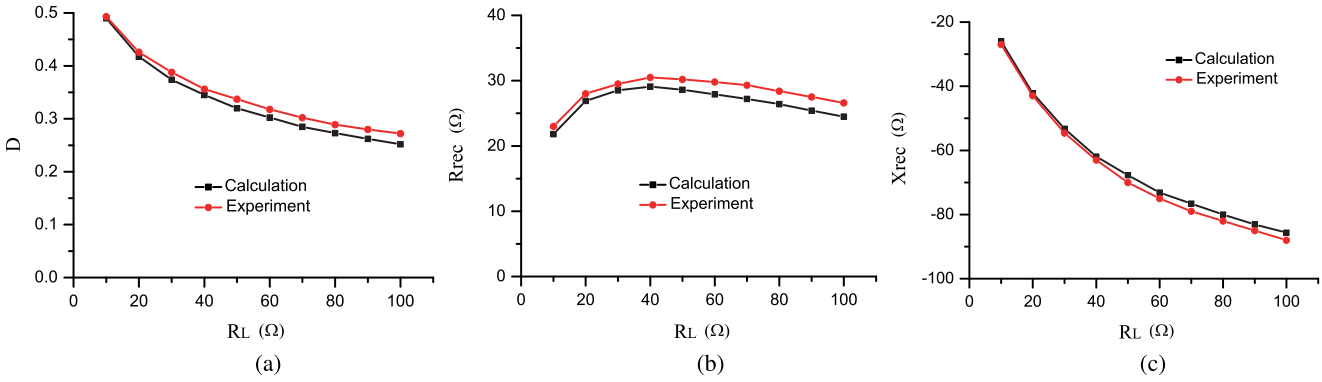

Fig. 10. Diode duty cycle and input impedance of the Class E full-wave rectifier. (a) Duty cycle. (b) $R_{\rm rec}$. (c) $X_{\rm rec}$.

ON for the rectification, thus a higher conduction loss occurs in the full-bridge rectifier. The power loss from the inductors in the full-wave rectifier is much smaller than the switching and conduction losses because the currents through the inductors L_1 and L_2 are the dc current $I_o/2$ and ESRs of the two dc filter inductors are very small. Therefore, the full-wave rectifier achieves a higher efficiency than that of the full-bridge rectifier even there is an additional power loss from the dc filter inductors L_1 and L_2.

The power factor can be used as an indication to show how reactive a circuit is to a power source. Since the output current of the series resonant receiving coil is sinusoidal, the power factors of the Class E full-wave rectifier and the full-bridge rectifier can be both expressed as follows in WPT systems:

$$\mathrm{PF}_{\rm rec} = \frac{P_{\rm rec}}{I_{\rm RMS} V_{\rm RMS}} = \frac{\sqrt{2} P_{\rm rec}}{I_m V_{\rm RMS}} \tag{28}$$

where $I_{\rm RMS}$ and $V_{\rm RMS}$ are the RMS of the input current and input voltage of the two rectifiers, and I_m is the amplitude of the input current. As shown in Fig. 8(b), the power factors of the two rectifiers both decrease with an increasing R_L. Note the power factor of the Class E full-wave rectifier is lower, but still larger than 0.4.

It is known that the power factor can also be represented as

$$\mathrm{PF} = \mathrm{PF}_{\rm dist} \cdot \mathrm{PF}_{\rm disp} \tag{29}$$

where $\mathrm{PF}_{\rm dist}$ is the distortion power factor and $\mathrm{PF}_{\rm disp}$ is the displacement power factor [38]. As shown in Table V, the full-wave rectifier is superior in the distortion power factor, while its smaller displacement power factor due to the larger reactance lowers the overall power factor of the rectifier [refer to Fig. 10(c)]. Again in order to compensate the large reactance of the Class E full-wave rectifier, system-level analysis and design are important to improve the efficiency and power transfer capability of the overall MHz WPT system [refer to Section III].

C. Voltage/Current Stress and Transfer Function

The ratio of the diode peak voltage/current to the output voltage/current ($V_{D,P}/V_o$ and $I_{D,P}/I_o$) can be used to evaluate the voltage/current stresses of the diodes, which are shown in Fig. 8(c) and (d), respectively. As shown in the figures, $V_{D,P}/V_o$ and $I_{D,P}/I_o$ of the Class E full-wave rectifier are higher than those of the full-bridge rectifier over a wide range of the load, which are caused by the sinusoidal input voltage in the full-wave rectifier. At the same time, the sinusoidal input voltage contributes to the lower harmonic contents in the full-wave rectifier and the overall WPT system. There is a tradeoff between the low harmonic contents and voltage/current stresses.

The voltage/current transfer functions are other important indices of the rectifiers to show the voltage/current gains from ac to dc. They are defined as the ratio of the output voltage/current of the rectifiers to the RMS of input voltage/current ($V_o/V_{\rm RMS}$ and $I_o/I_{\rm RMS}$). Fig. 8(e) and (f) shows the voltage/current transfer functions of the two rectifiers. It can be seen that the full-wave rectifier has a lower voltage transfer function than that of the full-bridge rectifier, and the current transfer function of the full-wave rectifier decreases when R_L increases. The lower voltage transfer function corresponds to a lower voltage gain of the full-wave rectifier. This may enable the dc load to be directly driven by the rectifier without the need of the step-down dc/dc conversion.

V. Experimental Results

A 10-W 6.78-MHz WPT system is built up to validate the previous analysis and design of the Class E full-wave current-driven rectifier, coupling coils, and the Class E PA, as shown in Fig. 9. Its configuration is as same as the circuit model in Fig. 6, and the design parameters in Table II are applied. In the experimental system, STPSC406 is used as the rectifying diode D_r, and SUD06N10 is for the switch of the PA. The parasitic capacitor of STPSC406 is assumed to be constant 35 pF, according to the datasheet, because the diode operates at a peak voltage around 60 V. Note again that the experimental results of the Class E full-wave rectifier and the full-bridge rectifier are both obtained when operating in the experimental WPT system. As shown in Fig. 9, the relatively large areas of the footprints in the coils are reserved for different connections of the discrete capacitors required in various experiments. In a final product, the areas can be largely reduced for a specific target application.

Fig. 10(a) shows the duty cycle of the Class E full-wave rectifier with the fixed C, 412 pF in Table II, and a varying

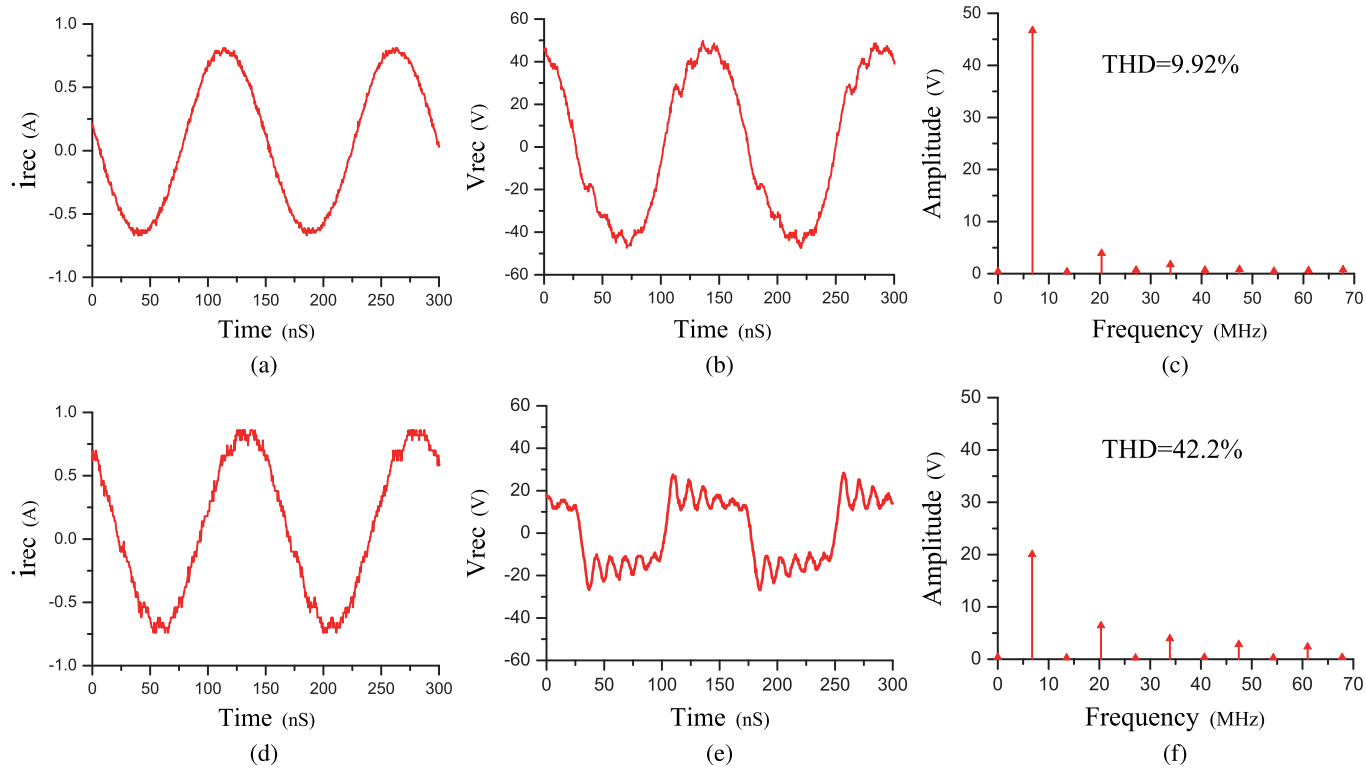

Fig. 11. Waveforms and harmonic contents. (a) Input voltage of full-wave rectifier. (b) Input current of full-wave rectifier. (c) Voltage harmonic contents of full-wave rectifier. (d) Input voltage of full-bridge rectifier. (e) Input current of full-bridge rectifier. (f) Voltage harmonic contents of full-bridge rectifier.

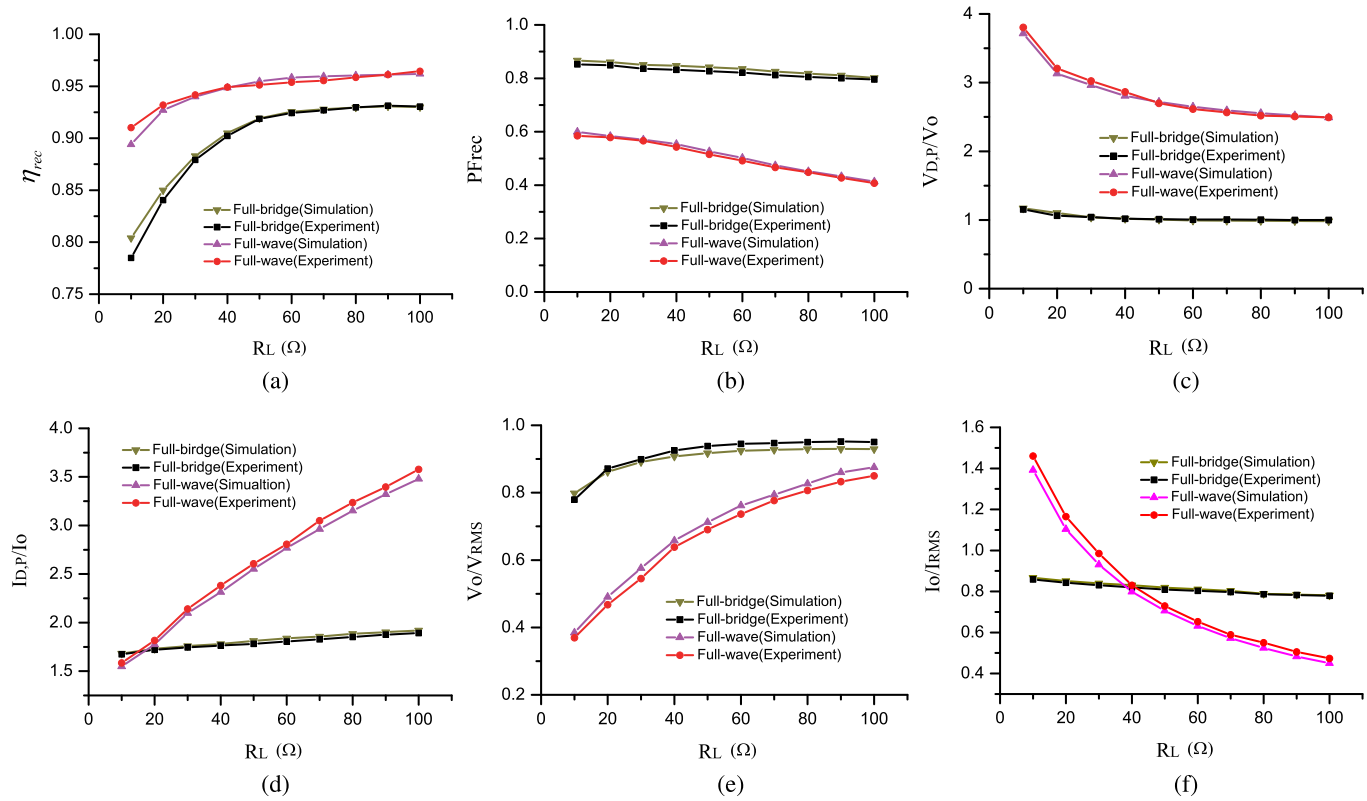

Fig. 12. Various parameters versus a varying R_L. (a) Efficiency. (b) Power factor. (c) Diode voltage stress. (d) Diode current stress. (e) Voltage transfer function. (f) Current transfer function.

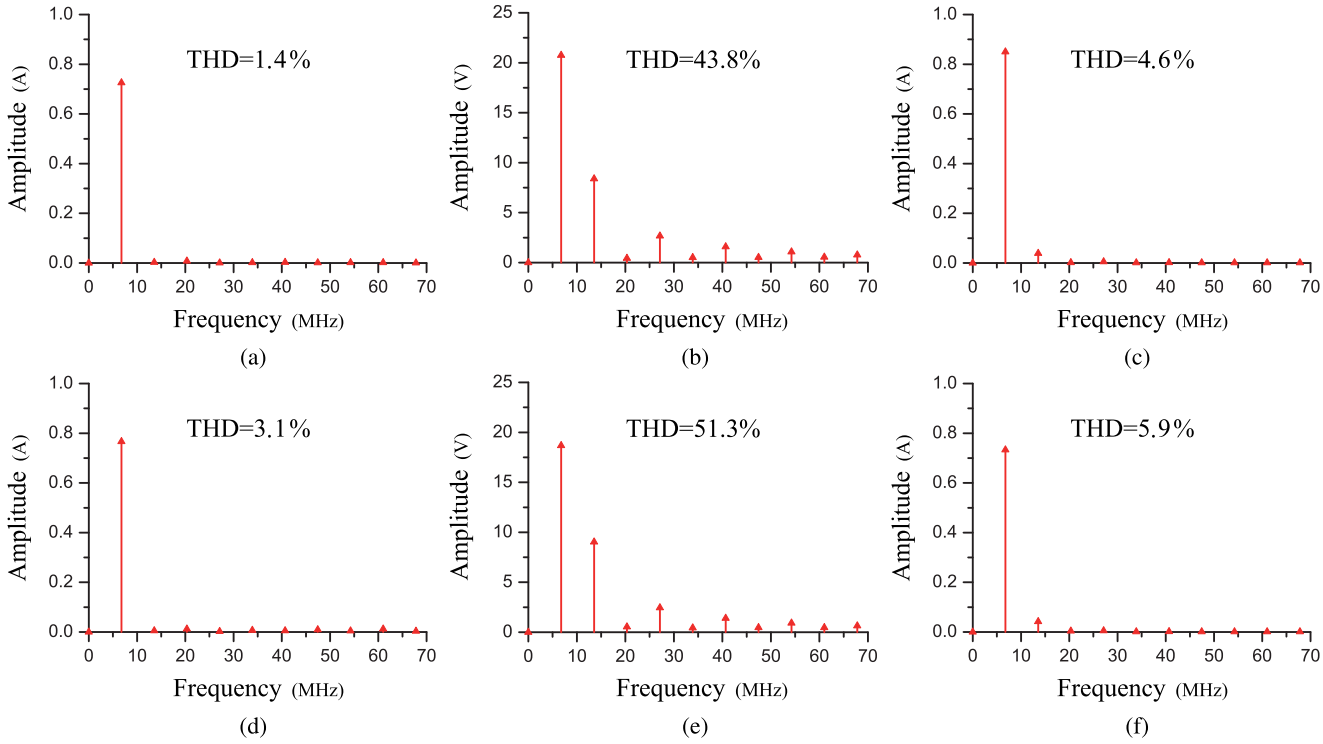

Fig. 13. THDs of the other three ac signals in the MHz WPT system. (a) Output current of the receiving coil using full-wave rectifier. (b) Input voltage of the transmitting coil using full-wave rectifier. (c) Input current of the transmitting coil using full-wave rectifier. (d) Output current of the receiving coil using full-bridge rectifier. (e) Input voltage of the transmitting coil using full-bridge rectifier. (f) Input current of the transmitting coil using full-bridge rectifier.

load R_L. The duty cycle decreases from 0.493 to 0.283 when R_L increases from 10 to 100 Ω. It validates the design of the rectifier to avoid the overlapping and maximize the power output capability, i.e., duty cycles around 0.5, over a wide range of load. Fig. 10(b) and (c) gives the experimental results, resistance, and reactance of the input impedance of the full-wave rectifier. The measured data is obtained through the fast Fourier transform of the raw data from the oscilloscope. In the above figures, the calculated results are also added, which well match the experimental results.

The experimental waveforms, harmonic contents, efficiency, power factor, diode voltage/current stresses, and voltage/current transfer functions of the Class E full-wave and conventional full-bridge rectifiers are shown in Figs. 11 and 12. The experimental results well match the simulation results in Figs. 7 and 8, and thus validate the previous theoretical analysis (the results in Fig. 8 are added in Fig. 12 for comparison purposes). As same as in simulation, the Class E full-wave rectifier shows higher efficiency over the full-bridge rectifier, while the power factor of the full-wave rectifier defined in (28) (> 0.4) is lower than that of the full-bridge rectifier. In the experiments, the efficiency and the power factor of the two rectifiers are calculated based on the voltage and current measurements. In order to achieve a high-accuracy measurement, the voltage and current probes are calibrated for a same phase at 6.78 MHz. Again due to the sinusoidal input voltage, the diode voltage/current stresses in full-wave rectifier are higher. However, the THD, 9.92%, of the full-wave rectifier is much lower than that of the conventional full-bridge rectifier, 42.2%. This advantage helps to improve the efficiency and EMI performance of the WPT system in real applications. In addition, as shown in Fig. 12(e), the voltage gain of the full-wave rectifier is lower than that of the full-bridge rectifier. This indicates that the full-wave rectifier is possible to drive the load directly without using a buck converter.

TABLE VI
LOSS BREAKDOWN OF RECTIFIERS IN EXPERIMENTS (RECTIFIER INPUT POWER $P_{\rm rec} = 10$ W; DC LOAD $R_L = 30$ Ω)

Loss	Full-wave Rec.	Full-bridge Rec.
$P_{\rm sw}$	0.26 W	0.61 W
$P_{\rm cd}$	0.29 W	0.60 W
P_L	0.03 W	-

In the present MHz WPT system, there are mainly four ac signals that largely affect the EMI performance of the final system, the input voltage/current of the transmitting coil, and the output voltage/current of the receiving coil (i.e., the input voltage/current of the rectifier). Besides Fig. 11(c) and (f), the THDs of the other three ac signals are further shown in Fig. 13(a)–(f). All the THDs are reduced by using the Class E full-wave rectifier. These THD measurements together indicate the improvement on the EMI performance of the overall MHz WPT system.

Table VI gives the experimental results on the loss breakdown of the full-wave and full-bridge rectifiers with a same 10 W input power of the rectifiers (i.e., $P_{\rm rec}$), again for a fair component-level comparison, and a target $R_L (= 30\ \Omega)$. Equations (23)–(27) are used to calculate the losses, but the dc output current

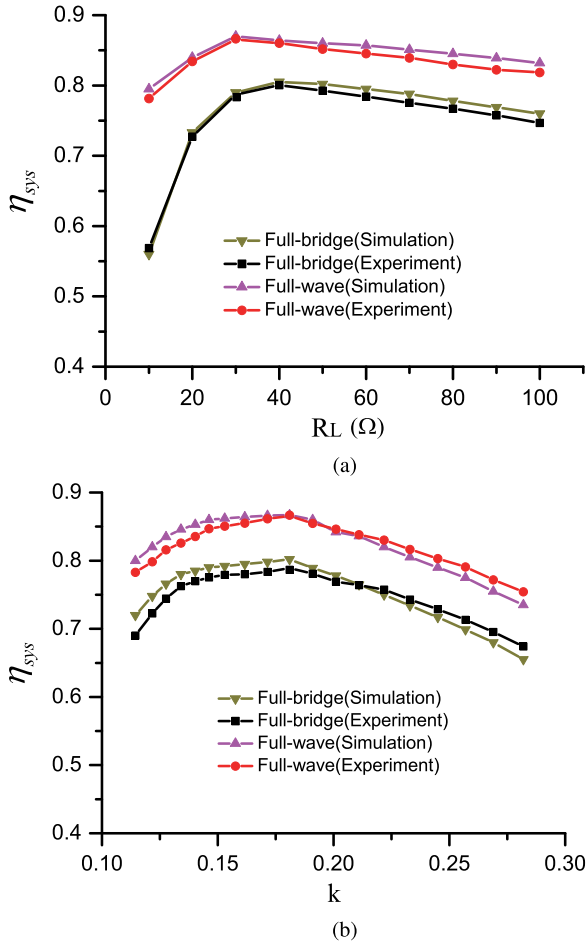

Fig. 14. Efficiencies comparison between the WPT systems using the proposed system design and the conventional design, respectively, when the Class E full-wave rectifier is used in both the WPT system. (a) Efficiencies versus R_L. (b) Efficiencies versus k (50–20 mm coil distances).

I_o and the diode currents i_{D_1} and i_{D_2} are the measured ones. Consistent with the simulation results and the analysis in Section IV-B, the full-wave rectifier shows a higher efficiency than that of the full-bridge rectifier.

Finally, for reference purposes, the system efficiencies of experiment and simulation $\eta_{\rm sys}$ versus R_L and k are shown in Fig. 14(a) and (b), respectively, for the WPT systems using the Class E full-wave rectifier and the full-bridge rectifier. Note the PA in the WPT system using the full-bridge rectifier is also optimized by (18) and (19). In the optimized design, the full-bridge rectifier is assumed to be purely resistive, which is a common practice. Here, V_{PA} is fixed as 22 V to achieve a 10-W power transfer under the target operating condition ($R_L = 30\ \Omega$ and $k = 0.18$). It can be seen that the WPT system using the full-wave rectifier achieves a higher efficiency than the WPT system using the conventional full-bridge rectifier over a wide range of R_L and k. The loss breakdown of the two systems is also listed in Table VII. For a system-level comparison, the input power of the two WPT systems $P_{\rm in}$ is same 10 W under $R_L = 30\ \Omega$ and $k = 0.18$. Thus, the rectifier input power $P_{\rm rec}$ is 9.25 and 8.88 W in the systems using the full-wave and full-bridge rectifiers, respectively, which are different with the condition in the previous Table VI. Table VII shows that the power losses from the rectifiers significantly affect the overall system efficiency in the two 6.78-MHz WPT systems. This justifies the use of the soft-switching-based Class E full-wave rectifier. It is especially interesting to note that the losses from the other components, the coupling coils and the PA, are also reduced in the WPT system using the full-wave rectifier, which validates the efforts of the system-level design and analysis discussed in this paper.

TABLE VII
LOSS BREAKDOWN OF SYSTEMS IN EXPERIMENTS (SYSTEM INPUT POWER $P_{\rm in} = 10$ W; DC LOAD $R_L = 30\ \Omega$)

Loss	WPT system (Full-wave Rec.)	WPT system (Full-bridge Rec.)
Rectifier	0.55 W	1.06 W
Coupling Coils	0.33 W	0.55 W
PA	0.42 W	0.65 W
Total	1.30 W	2.26 W

VI. CONCLUSION

This paper proposes the use of the Class E full-wave current-driven rectifier for a low-harmonic-contents and high-efficiency rectification in MHz WPT systems. Based on the input impedance of the rectifier, a design procedure is also developed to optimize the parameters of the Class E rectifier, coupling coils, and the PA. Both the simulation and experimental results show that the input voltage THD of the class E full-wave rectifier is significantly reduced to one-fourth of the THD of the conventional full-bridge rectifier. A high efficiency of the Class E full-wave rectifier, over 90%, is observed with a wide range of the load. The efficiency of the example 6.78-MHz WPT system is also improved to around 80% under a loosed coupling, $k = 0.18$. The results in this paper demonstrate the promising aspects of the Class E full-wave rectifiers in harmonic contents reduction and efficiency improvement when being applied in MHz WPT systems.

REFERENCES

[1] A. P. Hu, *Wireless/Contactless Power Supply:-Inductively Coupled Resonant Converter Solutions*. Saarbrücken, Germany: VDM, 2009.
[2] A. Kurs, A. Karalis, R. Moffatt, J. D. Joannopoulos, P. Fisher, and M. Soljačić, "Wireless power transfer via strongly coupled magnetic resonances," *Science*, vol. 317, no. 5834, pp. 83–86, Jul. 2007.
[3] P. Raval, D. Kacprzak, and A. Hu, "Multiphase inductive power transfer box based on a rotating magnetic field," *IEEE Trans. Ind. Electron.*, vol. 62, no. 2, pp. 795–802, Feb. 2015.
[4] D. Ahn and S. Hong, "Wireless power transfer resonance coupling amplification by load-modulation switching controller," *IEEE Trans. Ind. Electron.*, vol. 62, no. 2, pp. 898–909, Feb. 2015.
[5] S.-J. Huang, T.-S. Lee, and T.-H. Huang, "Inductive power transfer systems for PT-based ozone-driven circuit with flexible capacity operation and frequency-tracking mechanism," *IEEE Trans. Ind. Electron.*, vol. 61, no. 12, pp. 6691–6699, Dec. 2014.
[6] V. Prasanth and P. Bauer, "Distributed ipt systems for dynamic powering: Misalignment analysis," *IEEE Trans. Ind. Electron.*, vol. 61, no. 11, pp. 6013–6021, Nov. 2014.

[7] D. Ahn and S. Hong, "Wireless power transmission with self-regulated output voltage for biomedical implant," *IEEE Trans. Ind. Electron.*, vol. 61, no. 5, pp. 2225–2235, May 2014.
[8] S. Hui, W. Zhong, and C. Lee, "A critical review of recent progress in mid-range wireless power transfer," *IEEE Trans. Power Electron.*, vol. 29, no. 9, pp. 4500–4511, Sep. 2014.
[9] K. Shenai, "Accurate characterization of gate resistance and high-frequency switching efficiency of a power MOSFET," in *Proc. IEEE 21st Annu. Power Electron. Spec. Conf.*, San Antonio, TX, USA, Jun. 1990, pp. 107–112.
[10] C. Florian, F. Mastri, R. Paganelli, D. Masotti, and A. Costanzo, "Theoretical and numerical design of a wireless power transmission link with gan-based transmitter and adaptive receiver," *IEEE Trans. Microw. Theory Tech.*, vol. 62, no. 4, pp. 931–946, Apr. 2014.
[11] D. Ahn and P. Mercier, "Wireless power transfer with concurrent 200 kHz and 6.78 MHz operation in a single transmitter device," *IEEE Trans. Power Electron.*, vol. 31, no. 7, pp. 5018–5029, Jul. 2016.
[12] M. Fu, Z. Tang, M. Liu, C. Ma, and X. Zhu, "Full-bridge rectifier input reactance compensation in megahertz wireless power transfer systems," presented at the IEEE PELS Workshop Emerging Technologies, Wireless Power, Daejeon, Korea, Jun. 2015.
[13] W. Zhong, C. Zhang, X. Liu, and S. Hui, "A methodology for making a three-coil wireless power transfer system more energy efficient than a two-coil counterpart for extended transfer distance," *IEEE Trans. Power Electron.*, vol. 30, no. 2, pp. 933–942, Feb. 2015.
[14] M. Fu, T. Zhang, C. Ma, and X. Zhu, "Efficiency and optimal loads analysis for multiple-receiver wireless power transfer systems," *IEEE Trans. Microw. Theory Tech.*, vol. 63, no. 3, pp. 801–812, Mar. 2015.
[15] M. Pinuela, D. C. Yates, S. Lucyszyn, and P. D. Mitcheson, "Maximizing DC-to-load efficiency for inductive power transfer," *IEEE Trans. Power Electron.*, vol. 28, no. 5, pp. 2437–2447, May 2013.
[16] A. Sample, B. Waters, S. Wisdom, and J. Smith, "Enabling seamless wireless power delivery in dynamic environments," *Proc. IEEE*, vol. 101, no. 6, pp. 1343–1358, Jun. 2013.
[17] S.-H. Lee and R. D. Lorenz, "Development and validation of model for 95%-efficiency 220-W wireless power transfer over a 30-cm air gap," *IEEE Trans. Appl. Ind.*, vol. 47, no. 6, pp. 2495–2504, Nov. 2011.
[18] S. Aldhaher, P.-K. Luk, and J. F. Whidborne, "Electronic tuning of misaligned coils in wireless power transfer systems," *IEEE Trans. Power Electron.*, vol. 29, no. 11, pp. 5975–5982, Nov. 2014.
[19] S. Aldhaher, P.-K. Luk, A. Bati, and J. Whidborne, "Wireless power transfer using Class E inverter with saturable DC-feed inductor," *IEEE Trans. Ind. Appl.*, vol. 50, no. 4, pp. 2710–2718, Jul. 2014.
[20] P. Srimuang, N. Puangngernmak, and S. Chalermwisutkul, "13.56 MHz Class E power amplifier with 94.6% efficiency and 31 watts output power for RF heating applications," in *Proc. IEEE 11th Int. Conf. Electr. Eng./Electron., Comput., Telecommun. Inform. Technol.*, Nakhon Ratchasima, Thailand, May 2014.
[21] T. Suetsugu and M. Kazimierczuk, "Analysis and design of Class E amplifier with shunt capacitance composed of nonlinear and linear capacitances," *IEEE Trans. Circuits Syst.*, vol. 51, no. 7, pp. 1261–1268, Jul. 2004.
[22] M. Fu, H. Yin, X. Zhu, and C. Ma, "Analysis and tracking of optimal load in wireless power transfer systems," *IEEE Trans. Power Electron.*, vol. 30, no. 7, pp. 3952–3963, Jul. 2015.
[23] M. Fu, C. Ma, and X. Zhu, "A cascaded boost-buck converter for high efficiency wireless power transfer systems," *IEEE Trans. Ind. Informat.*, vol. 10, no. 3, pp. 1972–1980, Aug. 2014.
[24] T. Zhang, M. Fu, C. Ma, and X. Zhu, "Optimal load analysis for a two-receiver wireless power transfer system," in *Proc. IEEE Wireless Power Transfer Conf.*, Jeju, Korea, May 2014, pp. 84–87.
[25] M. Liu, M. Fu, and C. Ma, "Parameter design for a 6.78-MHz wireless power transfer system based on analytical derivation of class e current-driven rectifier," *IEEE Trans. Power Electron.*, vol. 31, no. 6, pp. 4280–4291, Jun. 2016.
[26] W. Nitz, W. Bowman, F. Dickens, F. Magalhaes, W. Strauss, W. Suiter, and N. Ziesse, "A new family of resonant rectifier circuits for high frequency DC-DC converter applications," in *Proc. IEEE 3rd Annu. Appl. Power Electron. Conf. Expo.*, New Orleans, LA, USA, Feb. 1988, pp. 12–22.
[27] A. Ivascu, M. Kazimierczuk, and S. Birca-Galateanu, "Class E resonant low dv/dt rectifier," *IEEE Trans.Circuits Syst. I, Fundam. Theory Appl.*, vol. 39, no. 8, pp. 604–613, Aug. 1992.
[28] M. Kazimierczuk and W. Szaraniec, "Analysis of a Class E rectifier with a series capacitor," *IEE Proc. G, Circuits, Devices Syst.*, vol. 139, no. 3, pp. 269–276, Jun. 1992.
[29] M. Kazimierczuk, "Class E low dv_D/dt rectifier," *IEE Proc. B, Electr. Power Appl.*, vol. 136, no. 6, pp. 257–262, Nov. 1989.
[30] J. Jozwik and M. Kazimierczuk, "Analysis and design of Class-E^2 DC/DC converter," *IEEE Trans. Ind. Electron.*, vol. 37, no. 2, pp. 173–183, Apr. 1990.
[31] Y. Minami and H. Koizumi, "Analysis of Class DE current driven low di/dt rectifier," *IEEE Trans. Power Electron.*, vol. 30, no. 12, pp. 6840–6816, Dec. 2015.
[32] A. Reatti, M. Kazimierczuk, and R. Redl, "Class E full-wave low dv/dt rectifier," *IEEE Trans.Circuits Syst. I, Fundam. Theory Appl.*, vol. 40, no. 2, pp. 73–85, Feb. 1993.
[33] S. Aldhaher, P.-K. Luk, K. El Khamlichi Drissi, and J. Whidborne, "High-input-voltage high-frequency Class E rectifiers for resonant inductive links," *IEEE Trans. Power Electron.*, vol. 30, no. 3, pp. 1328–1335, Mar. 2015.
[34] P.-K. Luk, S. Aldhaher, W. Fei, and J. Whidborne, "State-space modeling of a Class E^2 converter for inductive links," *IEEE Trans. Power Electron.*, vol. 30, no. 6, pp. 3242–3251, Jun. 2015.
[35] G. Kkelis, J. Lawson, D. Yates, M. Pinuela, and P. Mitcheson, "Integration of a Class-E low dv/dt rectifer in a wireless power transfer system," in *Proc. IEEE Wireless Power Transfer Conf.*, Jeju, Korea, May 2014, pp. 72–75.
[36] T. Nagashima, X. Wei, and H. Sekiya, "Analytical design procedure for resonant inductively coupled wireless power transfer system with Class-DE inverter and Class-E rectifier," in *Proc. Asia Pacific Conf. Circuits Syst.*, Melbourne, Vic., Australia, Nov. 2014, pp. 288–291.
[37] M. Albulet, *RF Power Amplifiers*. Raleigh, NC, USA: SciTech, 2001.
[38] G. J. Wakileh, *Power Systems Harmonics: Fundamentals, Analysis and Filter Design*. New York, NY, USA: Springer Science & Business, 2001.

Ming Liu (S'15) received the B.S. degree from SiChuan University, Sichuan, China, in 2007, and the M.S. degree from the University of Science and Technology Beijing, Beijing, China, in 2011, both in mechatronic engineering. He is currently working toward the Ph.D. degree in electrical and computer engineering at the University of Michigan-Shanghai Jiao Tong University Joint Institute, Shanghai Jiao Tong University, Shanghai, China.

His research interests include component- and system-level design of megahertz wireless power transfer systems and general power electronics systems.

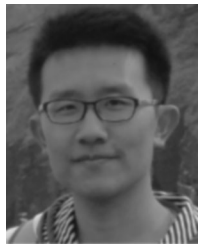

Minfan Fu (S'13) received the B.S. and M.S. degrees both in electrical and computer engineering from the University of Michigan-Shanghai Jiao Tong University Joint Institute, Shanghai Jiao Tong University, Shanghai, China, in 2010 and 2013, respectively, where he is currently working toward the Ph.D. degree.

His research interests include megahertz wireless power transfer, resonant converters, and circuit design optimization.

Chengbin Ma (M'05) received the B.S.E.E. (Hons.) degree from the East China University of Science and Technology, Shanghai, China, in 1997, and the M.S. and Ph.D. degrees both in the electrical engineering from the University of Tokyo, Tokyo, Japan, in 2001 and 2004, respectively.

He is currently an Assistant Professor of electrical and computer engineering at the University of Michigan-Shanghai Jiao Tong University Joint Institute, Shanghai Jiao Tong University, Shanghai. Between 2006 and 2008, he held a postdoctoral position with the Department of Mechanical and Aeronautical Engineering, University of California Davis, Davis, CA, USA. From 2004 to 2006, he was an R&D Researcher with Servo Laboratory, Fanuc Limited, Yamanashi, Japan. His research interests include wireless power transfer, networked hybrid energy system, electric vehicle, and mechatronic control.